



2-1999

# Parity Violation in Neutron Resonances in $^{107,109}\text{Ag}$

L Y. Lowie  
*North Carolina State University*

J D. Bowman  
*Los Alamos National Laboratory*

J Corvi  
*Institute for Reference Materials and Measurements*

*See next page for additional authors*

Follow this and additional works at: <https://cupola.gettysburg.edu/physfac>

 Part of the [Atomic, Molecular and Optical Physics Commons](#)

**Share feedback about the accessibility of this item.**

---

Lowie, L. Y., et al. (1999). Parity Violation in Neutron Resonances in  $^{107,109}\text{Ag}$ . *Physical Review C*, 59(2), 1119–1130.  
<http://dx.doi.org/10.1103/PhysRevC.59.1119>

This is the publisher's version of the work. This publication appears in Gettysburg College's institutional repository by permission of the copyright owner for personal use, not for redistribution. Cupola permanent link: <https://cupola.gettysburg.edu/physfac/16>

This open access article is brought to you by The Cupola: Scholarship at Gettysburg College. It has been accepted for inclusion by an authorized administrator of The Cupola. For more information, please contact [cupola@gettysburg.edu](mailto:cupola@gettysburg.edu).

---

# Parity Violation in Neutron Resonances in $^{107,109}\text{Ag}$

## Abstract

Parity nonconservation (PNC) was studied in p-wave resonances in Ag by measuring the helicity dependence of the neutron total cross section. Transmission measurements on natural Ag were performed in the energy range 32 to 422 eV with the time-of-flight method at the Manuel Lujan Neutron Scattering Center at Los Alamos National Laboratory. A total of 15 p-wave neutron resonances were studied in  $^{107}\text{Ag}$  and nine p-wave resonances in  $^{109}\text{Ag}$ . Statistically significant asymmetries were observed for eight resonances in  $^{107}\text{Ag}$  and for four resonances in  $^{109}\text{Ag}$ . An analysis treating the PNC matrix elements as random variables yields a weak spreading width of  $\Gamma_w = (2.67_{-1.21}^{+2.65}) \times 10^{-7}$  eV for  $^{107}\text{Ag}$  and  $\Gamma_w = (1.30_{-0.74}^{+2.49}) \times 10^{-7}$  eV for  $^{109}\text{Ag}$ .

## Keywords

parity nonconservation, neutron resonances

## Disciplines

Atomic, Molecular and Optical Physics | Physics

## Authors

L Y. Lowie, J D. Bowman, J Corvi, Bret E. Crawford, P P J. Delheij, C M. Frankle, M Inuma, J N. Knudsen, A Masaike, Y Matsuda, G E. Mitchell, S I. Penttila, H Postma, N R. Roberson, S J. Seestrom, E I. Sharapov, and H M. Shimizu

## Parity violation in neutron resonances in $^{107,109}\text{Ag}$

L. Y. Lowie,<sup>1,\*</sup> J. D. Bowman,<sup>2</sup> F. Corvi,<sup>3</sup> B. E. Crawford,<sup>4,†</sup> P. P. J. Delheij,<sup>5</sup> C. M. Frankle,<sup>2</sup> M. Iinuma,<sup>6,‡</sup> J. N. Knudson,<sup>2</sup> A. Msaïke,<sup>6</sup> Y. Masuda,<sup>7</sup> Y. Matsuda,<sup>6,§</sup> G. E. Mitchell,<sup>1</sup> S. I. Penttilä,<sup>2</sup> H. Postma,<sup>8</sup> N. R. Roberson,<sup>4</sup> S. J. Seestrom,<sup>2</sup> E. I. Sharapov,<sup>9</sup> H. M. Shimizu,<sup>6,§</sup> S. L. Stephenson,<sup>1,||</sup> Y.-F. Yen,<sup>2,¶</sup> V. W. Yuan,<sup>2</sup> and L. Zanini<sup>3</sup>

<sup>1</sup>North Carolina State University, Raleigh, North Carolina 27695-8202

and Triangle Universities Nuclear Laboratory, Durham, North Carolina 27708-0308

<sup>2</sup>Los Alamos National Laboratory, Los Alamos, New Mexico 87545

<sup>3</sup>Institute for Reference Materials and Measurements, Geel, Belgium

<sup>4</sup>Duke University, Durham, North Carolina 27708

and Triangle Universities Nuclear Laboratory, Durham, North Carolina 27708-0308

<sup>5</sup>TRIUMF, Vancouver, British Columbia, Canada V6T 2A3

<sup>6</sup>Department of Physics, Kyoto University, Kyoto 606-01, Japan

<sup>7</sup>National Laboratory for High Energy Physics, 1-1, Oho, Tsukuba 305, Japan

<sup>8</sup>Delft University of Technology, Delft, 2600 GA, The Netherlands

<sup>9</sup>Joint Institute for Nuclear Research, 141980 Dubna, Russia

(Received 19 August 1998)

Parity nonconservation (PNC) was studied in  $p$ -wave resonances in Ag by measuring the helicity dependence of the neutron total cross section. Transmission measurements on natural Ag were performed in the energy range 32 to 422 eV with the time-of-flight method at the Manuel Lujan Neutron Scattering Center at Los Alamos National Laboratory. A total of 15  $p$ -wave neutron resonances were studied in  $^{107}\text{Ag}$  and nine  $p$ -wave resonances in  $^{109}\text{Ag}$ . Statistically significant asymmetries were observed for eight resonances in  $^{107}\text{Ag}$  and for four resonances in  $^{109}\text{Ag}$ . An analysis treating the PNC matrix elements as random variables yields a weak spreading width of  $\Gamma_w = (2.67_{-1.21}^{+2.65}) \times 10^{-7}$  eV for  $^{107}\text{Ag}$  and  $\Gamma_w = (1.30_{-0.74}^{+2.49}) \times 10^{-7}$  eV for  $^{109}\text{Ag}$ . [S0556-2813(99)03102-7]

PACS number(s): 24.80.+y, 25.40.Ny, 27.60.+j, 11.30.Er

### I. INTRODUCTION

In the standard approach to parity nonconservation (PNC) in light nuclei, parity doublets (closely spaced, low-lying states of the same angular momentum and opposite parity) are studied. A parity-forbidden observable is measured and the wavefunctions for the initial and final states calculated as well as possible. After the discovery [1] of very large enhancement of parity violation for neutron resonances in heavy nuclei, a statistical ansatz was adopted: the compound nucleus is considered a statistical system and the symmetry-breaking matrix elements as random variables. In this approach the result of a PNC experiment is the root-mean-square symmetry-breaking matrix element. The different viewpoints are illustrated by the differences between the classic review by Adelberger and Haxton [2] (where the

PNC measurements in nucleon-nucleon scattering and the PNC data from light nuclei are compared with the predictions of Desplanques, Donoghue, and Holstein [3]) and the recent reviews by Bowman *et al.*, [4] Frankle *et al.*, [5] and Flambaum and Gribakin [6].

In the early neutron resonance experiments only one parity violation was measured per nuclide. This was a crucial limitation, since several experimental parity violations are required for the statistical analysis. The Time Reversal Invariance and Parity at Low Energies (TRIPLE) Collaboration initiated a program to study parity violation for a number of resonances in each nuclide, using the high neutron flux available at the Manuel Lujan Neutron Scattering Center at the Los Alamos Neutron Science Center (LANSCE). In our initial measurements the TRIPLE Collaboration measured a number of parity violations in  $^{238}\text{U}$  [7,8] and  $^{232}\text{Th}$  [9,10]. To improve the quality of the data, we redesigned and rebuilt essentially every component of the experimental system and then remeasured parity violations in  $^{238}\text{U}$  [11] and  $^{232}\text{Th}$  [12]. All of the initial measurements were near the maximum of the  $4p$  neutron strength function, and thus gave no information concerning any mass dependence in the effective nucleon-nucleus weak interaction. In addition, there was a nonstatistical effect observed in  $^{232}\text{Th}$ , where ten parity violations in a row all had the same sign, thus apparently contradicting the statistical assumption. It is very important to determine whether this nonstatistical effect is general or limited to  $^{232}\text{Th}$ .

\*Present address: McKinsey and Company, Atlanta, GA 30303.

†Present address: North Carolina State University, Raleigh, NC 27695-8202 and Gettysburg College, Gettysburg, PA 17325.

‡Present address: Hiroshima University, Hiroshima-Ken 739-8526, Japan.

§Present address: Institute of Physical and Chemical Research (RIKEN), Saitama, 351-0198, Japan.

||Present address: Gettysburg College, Gettysburg, PA 17325.

¶Present address: Wake Forest University School of Medicine, Winston-Salem, NC 27157.

In practice the parity violation measurements are feasible only near a maximum of the  $p$ -wave neutron strength function. Therefore our attention turned to the mass  $A = 110$  region, where the  $3p$  neutron strength function maximum is located. The size of the experimental PNC effect is proportional to the level density, and on average for even-even targets the level density is smaller near  $A = 110$  than  $A = 230$ . Therefore we studied odd mass targets. In addition, many even-even nuclei in this mass region are not available in the large quantity needed for the transmission experiment. This approach was successful, in the sense that many PNC effects were observed, for almost all odd mass targets that we have studied near the  $3p$  neutron strength function maximum. However, a complication arises in the analysis of these data. As we discuss below, it is important to have spectroscopic information (including spins) for the  $s$ - and  $p$ -wave resonances. Absent such spectroscopic information one can proceed by averaging over the various possibilities, but this often introduces a large uncertainty into the value for the rms PNC matrix element.

In this paper we report PNC measurements on  $^{107}\text{Ag}$  and  $^{109}\text{Ag}$ . These measurements formed part of the thesis of Lowie [13]. In addition, we present the results of spin determination measurements performed at the Institute for Reference Materials and Measurements (IRMM). These latter measurements formed part of the thesis of Zanini [14] and were also reported in Refs. [15,16].

We define the PNC asymmetry  $p$  for an  $l = 1$  ( $p$ -wave) resonance from  $\sigma_p^\pm = \sigma_p(1 + p^\pm)$ , where  $\sigma_p^\pm$  is the resonance cross section for  $+$  and  $-$  helicities,  $\sigma_p$  is the resonance part of the  $p$ -wave cross section, and here the neutron polarization is assumed to be one. (The neutron polarization is monitored throughout and the polarization value incorporated in the detailed analysis.) The spirit of the analysis approach is that the resonance parameters are determined (with a multilevel, multichannel code described below), and that these resonance parameters are then held fixed while the longitudinal asymmetries are determined separately for the  $+$  and  $-$  helicity states. After the neutron resonance parameters are determined, including the resonance cross section  $\sigma_p$  for the  $p$ -wave resonance in question, the asymmetry parameters  $p^\pm$  are determined from  $\sigma_p^\pm$ . The longitudinal asymmetry  $p$  is then determined from  $p = (\sigma_p^+ - \sigma_p^-) / (\sigma_p^+ + \sigma_p^-) = (p^+ - p^-) / (2 + p^+ + p^-)$ .

The experimental system for the parity violation measurements is described in Sec. II A and the experimental system for the spin determinations in Sec. II B. The experimental data for the parity violation experiment and the analysis to determine the resonance strengths and the longitudinal asymmetries are discussed in Sec. III A. The data for spin determination and the method of analysis are described in Sec. III B. In Sec. IV the results for the resonance spectroscopy are presented. Section V describes the analysis to determine the rms matrix element, emphasizing the importance of the resonance spectroscopy. The PNC longitudinal asymmetries are presented in Sec. VI, along with the rms PNC matrix elements. A brief summary is given in the final section.

## II. EXPERIMENTAL METHODS

### A. Parity violation

To produce the intense epithermal neutron beam at the Manuel Lujan Neutron Scattering Center, 800-MeV protons

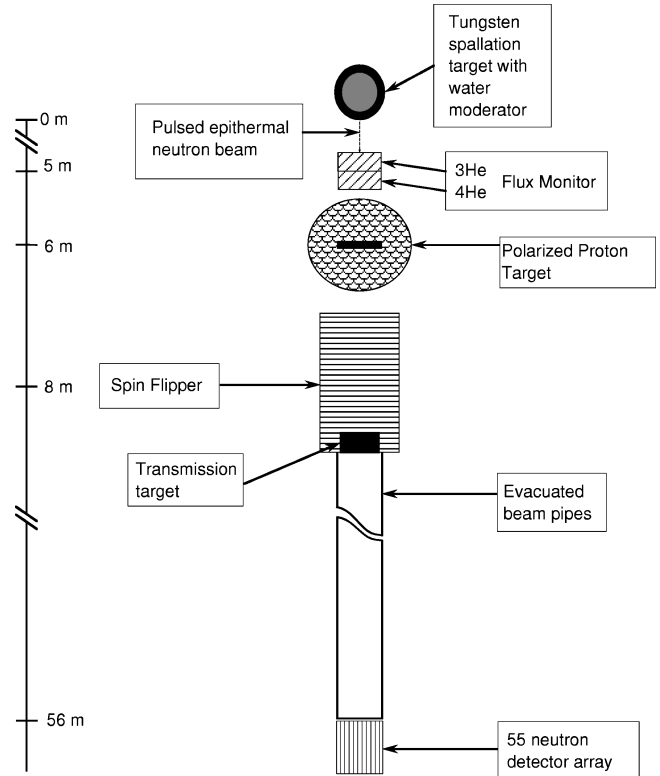


FIG. 1. Overview of the polarized neutron flight path at the Manuel Lujan Neutron Scattering Center.

from the LANSCE linac are chopped to 250-ns wide pulses separated by 110 ns. The proton bunches are injected into the Proton Storage Ring (PSR), which has a transit time of 360 ns. The proton bunches are stacked on top of one another and accumulated in the PSR. The resulting proton pulses have the shape of an isosceles triangle of base 250 ns and separated by 50 ms. The accumulated proton beam (typically  $70 \mu\text{A}$  for this experiment) is then directed towards a tungsten spallation target, and approximately 17 neutrons are produced for each incident proton. The neutrons are then moderated and collimated. A detailed description of the target-moderator geometry is given by Lisowski *et al.* [17].

An overview of the TRIPLE Collaboration experimental setup as used in our first experiments was given by Roberson *et al.* [18]. Crawford *et al.* [11] describe the improvements since the earlier work. An overview of the TRIPLE experimental system is shown in Fig. 1.

As the neutron beam enters the TRIPLE beam line, the flux is monitored by a pair of ionization chambers [19]. The neutron beam is polarized by transmission through a polarized proton target. The protons are polarized in a frozen ammonia target with the dynamic polarization method [20,21]. The target is cooled in liquid  $^4\text{He}$  to 1 K at the center of a 5-T split-coil superconducting magnet. The proton polarization was monitored with a nuclear magnetic resonance (NMR) measurement. The NMR measurement provides a rapid *relative* determination of the proton polarization. Methods of determining the absolute polarization are discussed by Yuan *et al.* [22]. In practice the typical neutron polarization was about 70%. The spin direction of the neutrons could be adiabatically reversed by a ‘‘spin flipper’’ consisting of a

series of longitudinal and transverse magnetic fields [23]. An additional reversal of the spin direction could be performed with the two different microwave transition frequencies that polarize the protons parallel or antiparallel to the magnetic field direction, so that only the microwave frequency needs to be changed and not the magnetic field direction. Changing the proton polarization direction provides a second convenient way to check for possible systematic errors. Since this change takes 1–2 h, it is performed only a few times during the 1–2 weeks it takes to study PNC in a typical target.

The neutron detector system consists of 55 photomultiplier tubes (PMTs) optically coupled to a liquid scintillator ( $C_{11}H_{10}+C_3H_9BO$ ) loaded with  $^{10}B$  [24]. The scintillator is segmented into 55 cells arranged in a honeycomb pattern with each cell viewed by a PMT on the downstream side of the detector, which is located at 57 m. This detector allows very high instantaneous counting rates and has a very high and nearly energy-independent efficiency.

The data acquisition process is initiated with each proton burst. The detector signals are linearly summed and filtered. An ADC transient recorder digitally samples the summed detector signal 8192 times in intervals determined by the filtering time. The 8192 words are added to a summation memory for 200 beam bursts before being stored.

The neutron spin direction is changed by the spin flipper according to an eight-step sequence designed to reduce the effects of gain drifts and residual transverse magnetic fields [18]. The transverse field of the spin flipper is off (spin is not reversed) or on (spin is reversed) according to the following sequence  $0+ +0-00-$ , where 0 indicates that the transverse field is off, and  $\pm$  that the transverse field is on in the up or down transverse direction. Each spin flipper state lasts 10 s (200 beam pulses). After 20 eight-step sequences have been performed, the data from this approximately 30-min collection period are stored for later analysis. The result is a large number of small data sets (called ‘runs’) during which the experimental conditions should be relatively constant. These runs are analyzed separately.

**B. Spin determination**

Measurements to determine resonance spins were performed at the GELINA pulsed neutron source facility using the time-of-flight technique [14]. The Geel Linac and associated compressing magnet were operated to provide electron bursts of 100-MeV average energy and 1-ns width at a repetition frequency of 800 Hz and an average beam current of about  $75 \mu A$ . Neutrons produced by bremsstrahlung  $\gamma$  rays inside the rotating uranium target were subsequently moderated in two 4-cm thick water slabs canned in beryllium. The neutron beam was filtered afterwards by a natural  $B_4C$  sample of thickness  $0.335 \text{ g/cm}^2$  to absorb slow neutrons from the previous cycles. A 2-cm thick lead disc was inserted in order to reduce the effects of the  $\gamma$  flash on the detection system. The two samples used were both on loan from the ORNL Isotope Pool. The  $^{107}Ag$  sample was enriched to 98.3%  $^{107}Ag$  and consisted of 49.8 g in the form of a silver metal powder disc of diameter 8.9 cm, packed in an aluminum box with walls 0.05-cm thick. The  $^{109}Ag$  sample was enriched to 97.1%  $^{109}Ag$  and consisted of 49.9 g in the form of a silver metal disc of 10-cm diameter. The samples

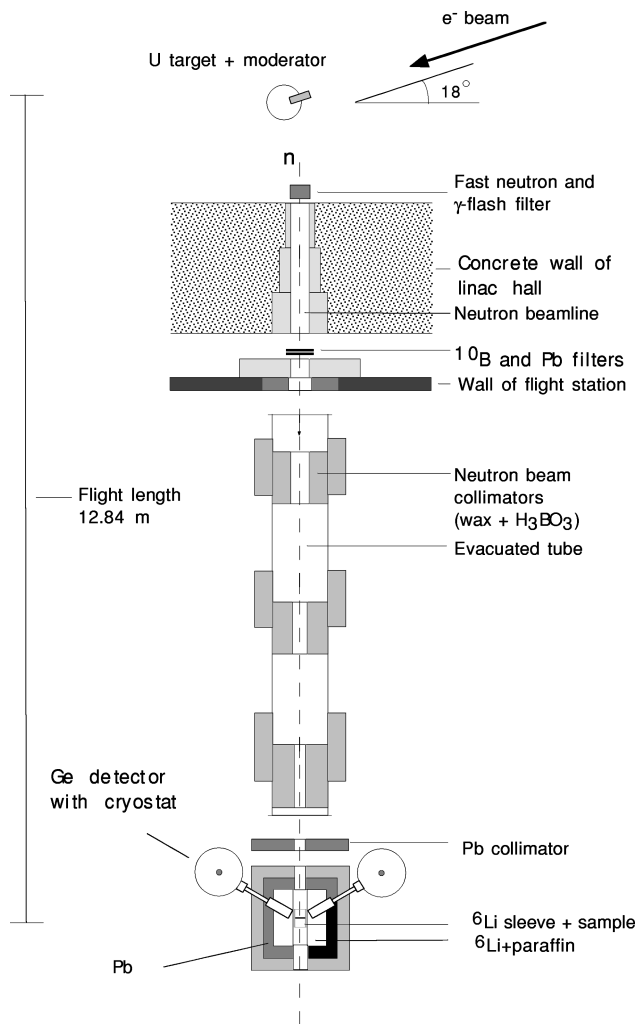


FIG. 2. Experimental arrangement for the capture  $\gamma$ -ray experiments at the GELINA pulsed neutron source.

were placed perpendicular to the beam at a flight distance of 12.85 m. The experimental system is shown schematically in Fig. 2. Neutron capture  $\gamma$  rays were detected by two coaxial intrinsic Ge crystals of 70% efficiency (relative to the  $^{60}Co$  line), placed at a distance of 15 cm from the sample center and at  $120^\circ$  with respect to the neutron direction. In order to prevent detection of scattered neutrons, 4-cm thick discs made of wax and  $^6Li$  carbonate were inserted between sample and detector. The entire structure was contained inside a shielding made of lead and borated wax each 10-cm thick.

The amplitude information from the Ge detectors was measured with two 8k fast ADCs for the  $\gamma$ -ray energy range 0.1–7.2 MeV, in coincidence with the time-of-flight (TOF) information, measured with a 25-bit multiple shot time digitizer. These events were recorded in event mode on the 1-Gbyte hard disk of a PC-based data acquisition system. The event-mode data were sorted on an Exabyte tape unit for subsequent processing with a Macintosh PC. For  $^{107}Ag$ , the neutron energy range from 10 to 800 eV was covered and a total of 27 Gbytes of event-mode data were collected over a period of 900 h. For  $^{109}Ag$ , the neutron energy range was from 10 to 1400 eV, with a total of 40 Gbytes of data measured over a period of 1200 h.

### III. PNC EXPERIMENTAL DATA AND ANALYSIS DESCRIPTION

#### A. Parity violation data and analysis to obtain asymmetry

The target was a cylinder of natural silver (2986 g, 99.999% chemical purity) 10.5 cm in diameter and length 8.6 cm. The silver sample was located at the exit of the neutron spin rotation device, approximately 9.7 m from the neutron source. After preliminary evaluation of the spectra, a total of 258 runs were selected to be used in the analysis. Background and dead time corrections were applied as described by Crawford *et al.* [11] and Stephenson *et al.* [12].

The code FITXS [25] was written specifically to analyze the TOF spectra measured by the TRIPLE Collaboration. For a particular time-of-flight region and a set of fitting parameters, the  $\chi^2$  is minimized to obtain the optimum set of parameter values. The fitting function depends on the target areal density  $n$ , the multilevel cross sections, and broadening due to three sources: the neutron beam, Doppler broadening, and the detector system. The broadening due to the beam and the detection system can be combined to form a response function  $B_i(t)$ .

For this transmission experiment, the fitting function can be written as

$$\mathcal{F}_i(t) = B_i(t) \otimes [N_0(t) e^{-n\sigma_D(t)}] + \mathcal{B}, \quad (1)$$

where

$$\sigma_D(t) = [D(v) \otimes \sigma(v)]_{v \rightarrow t}, \quad (2)$$

$N_0$  is the neutron flux,  $D(v)$  is the Doppler response function,  $\mathcal{B}$  is the background function, and the  $v \rightarrow t$  symbol indicates that after the convolution in velocity space, the cross section is converted to a function of time. The convolutions in Eq. (1) do not commute.

In our analysis approach the neutron cross section data are fit first, and then the longitudinal asymmetries are determined with all of the resonance parameters held fixed. The multilevel, multichannel neutron cross section is calculated with the formalism of Reich and Moore [26]. We adopt the following notation: the resonance energy is  $E_{s,p}$ , the neutron width  $\Gamma_n^{s,p}$ , and the total width  $\Gamma^{s,p}$ . Expressions for the  $s$ - and  $p$ -wave cross sections are given by Crawford *et al.* [11]. The final expression for  $B_i(t)$  includes the measured beam response (determined by fits to a spectrum obtained with a capture detector at energies where the beam response dominates) and additional broadening from the neutron detector.

Including an energy-dependent flux and allowing for background (described by a polynomial in time), the final fitting function can be written as

$$\mathcal{F}_i(t) = \left\{ B_i(t) \otimes \left[ \frac{\alpha}{E^\beta} e^{-n\sigma_D(t)} \right] \right\} + \sum_{i=0}^3 \frac{a_i}{t^i}, \quad (3)$$

where  $\sigma_D(t)$  is the Doppler-broadened total cross section for  $s$ - and  $p$ -wave resonances. The  $s$ - and  $p$ -wave cross sections are calculated for all resonances present (including contaminants) and summed to form the total elastic and capture cross sections. A sample multilevel fit is shown in Fig. 3.

When a final satisfactory fit is obtained for a given energy region, all of the resonance parameters are held fixed and the

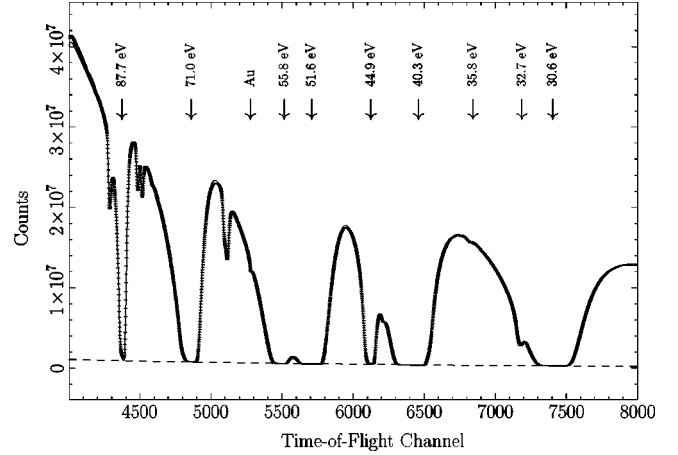


FIG. 3. Sample multilevel fit to the natural silver time-of-flight spectrum in the energy region 30 – 150 eV.

longitudinal asymmetry varied. This is performed for each helicity state for each run. The neutron polarization is determined for each run and the correction made for the polarization. (The observed asymmetry is the product of the neutron polarization and the true asymmetry.) The asymmetry values are then corrected for the spin-flipping efficiency which is a function only of neutron energy. These final asymmetry values are then used to determine a mean value of the asymmetry and its error. The results for two resonances are shown in Fig. 4. The uncertainty in the mean value of  $p$  is the variance of the histogram divided by  $N^{1/2}$ . The histograms for all of the resonances are approximately Gaussian.

#### B. Spin and parity assignments

In order to determine the resonance spins, the low-level population method of spin assignment was used. This tech-

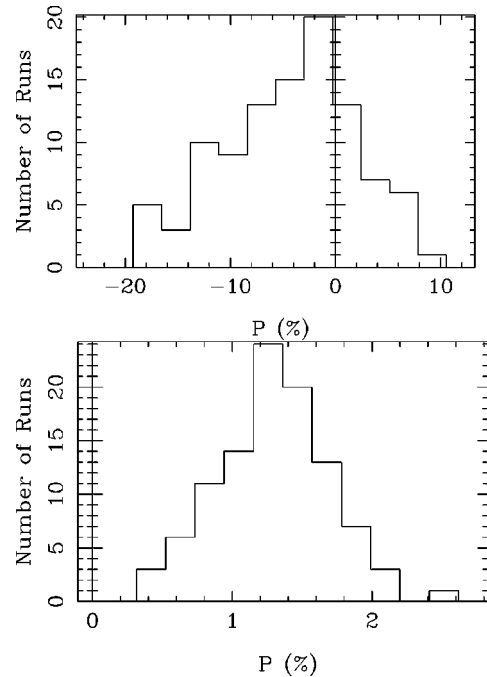


FIG. 4. Top: Histogram of the asymmetries obtained for 152 runs for the 36-eV resonance in  $^{107}\text{Ag}$ . Bottom: Histogram of the asymmetries obtained for 152 runs for the 32-eV resonance in  $^{109}\text{Ag}$ .

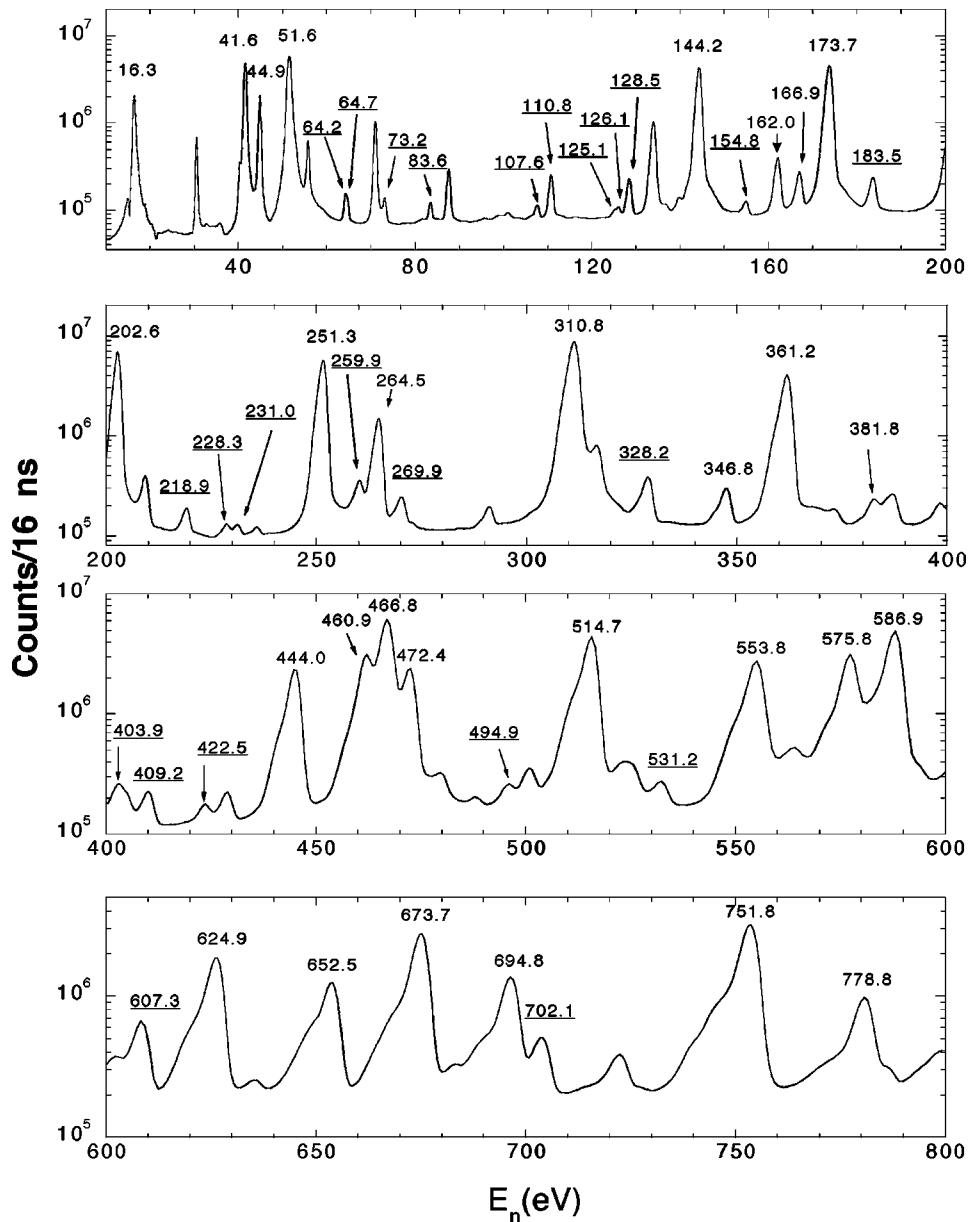


FIG. 5. Time-of-flight spectrum for  $^{107}\text{Ag}(n, \gamma)$ . The  $p$ -wave resonance energies are underlined.

nique exploits the fact that the population of excited states reached by radiative neutron capture depends significantly on the initial spin. This property holds for all nuclides whose decay can be treated statistically, i.e., when the level density and therefore the number of possible  $\gamma$ -ray cascades is high. In the past the method was successfully applied to a number of nuclei to determine the spins of  $s$ -wave resonances. The extension to the  $p$ -wave resonance case is straightforward, although experimentally more difficult because of the weak strength of most  $p$ -wave resonances.

The spin effect is mainly based on two characteristics of the radiative decay. First, dipole transitions predominate (for each dipole step of the cascade, the difference between initial and final spin is zero or one). Second, the  $\gamma$ -ray multiplicity is small. It follows that the smaller the spin difference between the neutron resonance and a given final state of the cascade, the larger the population of the final state.

The relative populations of the excited states are determined by measuring the intensities of  $\gamma$ -ray transitions deex-

citing them. In order to increase the sensitivity of the method and also to avoid normalization problems for the different resonances, it is convenient to measure the intensity ratio of two transitions depopulating levels of different spin. Usually a larger spin difference leads to a larger effect. The transitions chosen should conform to this rule and also should be strong enough to be observed in most  $p$ -wave resonances.

From the recorded data, 149 capture  $\gamma$ -ray spectra (corresponding to as many TOF intervals) were sorted for  $^{107}\text{Ag}$  and 138 spectra for  $^{109}\text{Ag}$ . These TOF intervals correspond either to a single neutron resonance or to a background region between resonances. After normalization, the  $\gamma$ -ray spectrum corresponding to one or more background regions was subtracted from the raw data. The TOF spectrum for  $^{107}\text{Ag}$  in the energy range 10 to 800 eV is shown in Fig. 5. The energies of the resonances analyzed are indicated. The  $p$ -wave resonance energies are underlined. Low-energy  $\gamma$ -ray spectra for five  $^{107}\text{Ag}$  resonances of different spin and parity are shown in Fig. 6. One notes that the transitions at

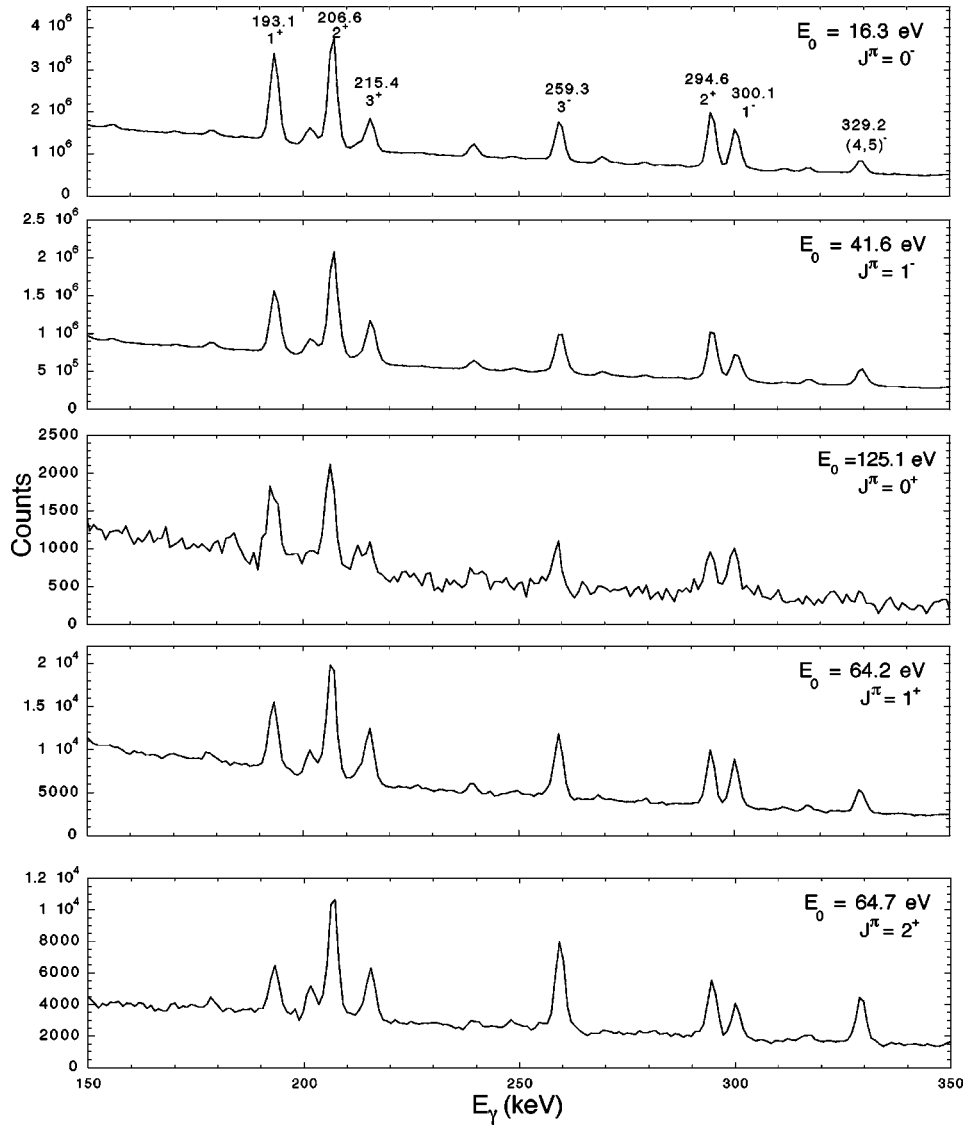


FIG. 6. Low-energy  $\gamma$ -ray spectra for five  $^{107}\text{Ag}$  resonances of different spin and parity; the energies of the strongest transitions and the spins and parities of their initial levels are indicated.

215.4-, 259.3-, and 329.2-keV, depopulating levels with spins ranging from 3 to 5, are progressively stronger in resonances with  $J=0, 1$ , and 2. The opposite happens for transitions at 193.1- and 300.1-keV, depopulating levels with  $J=1$ .

The energies of the stronger transitions are indicated, along with the spin and parity of the state from which the transition originates. In Fig. 7 the intensity ratios between the  $\gamma$ -ray transitions of 300.1- and 329.2-keV are plotted versus the energy of the  $^{107}\text{Ag}$   $s$ - and  $p$ -wave resonances. The separation in two and three spin groups, respectively, is distinctive, allowing a  $J$  assignment. In the same manner, assignments were obtained for  $^{109}\text{Ag}$  resonances using the ratio of the intensities of the  $\gamma$ -ray transitions (235.7 + 237.1 keV) and 191.5 keV.

The standard method to determine the orbital angular momentum for low energy neutron resonances uses the Bayesian method developed by Bollinger and Thomas [27]. This method relies on the fact that the difference in penetrabilities for the  $s$ - and  $p$ -wave resonances is so large that most of the weaker resonances are  $p$  wave and most of the stronger reso-

nances are  $s$  wave. This method works well in practice and was applied in this case. However, it is also interesting to ask whether the radiative decay patterns show a ‘‘parity’’ effect analogous to the ‘‘spin’’ effect described above. In an attempt to separate the resonance sample into two groups with  $l=0$  and  $l=1$ , for  $^{107}\text{Ag}$  we considered the ratio of the sum of the intensities for the two transitions (259.3 + 300.1 keV), deexciting negative parity low-lying states, and the intensity of the 294.6-keV transition, deexciting a positive parity state [16]. In Fig. 8 this intensity ratio is plotted for all  $^{107}\text{Ag}$  resonances. A net separation is evident between the two parities. For the  $^{109}\text{Ag}$  resonances we used the ratio between the intensities of the sum of the 235.7- and 237.1-keV transitions and the 198.7-keV transition. Parity assignments by the two methods agree in all cases except for the 166.9-, 346.8-, and 391.8-eV resonances in  $^{107}\text{Ag}$  and the 106.3 and 169.8-eV resonances in  $^{109}\text{Ag}$ . In these cases we gave preference (in Tables I and II) to the  $\gamma$ -ray assignment. More detailed discussion is given by Zanini *et al.* [15].

Additional information on the resonance spins can be obtained from the primary transitions to low-lying states of a

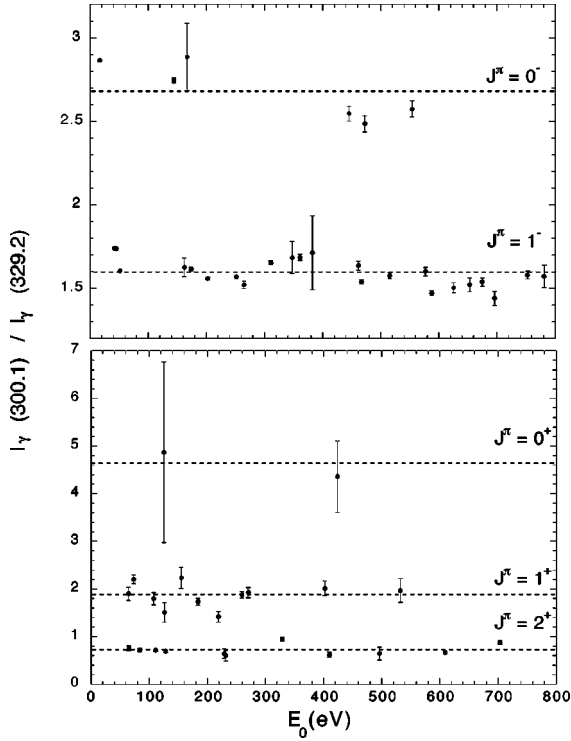


FIG. 7. Intensity ratios between the indicated  $\gamma$ -ray transitions plotted versus neutron energy for  $s$ - and  $p$ -wave resonances in  $^{107}\text{Ag}$ ; (top)  $s$ -wave resonances with spins  $J^\pi=0^-$  and  $1^-$ , (bottom)  $p$ -wave resonances with spins  $J^\pi=0^+$ ,  $1^+$ , and  $2^+$ . The dotted lines are the means of the various groups.

given spin. For example, both isotopes studied in the present paper have spin and parity  $I^\pi=1/2^-$ , leading to  $s$ -wave resonances with  $J^\pi=0^-$  or  $1^-$ . Based on electromagnetic selection rules, the observation of primary transitions to low-lying states of known spin and parity can also provide information on  $J$  and/or  $\pi$  of the initial states. Such primary transitions can only be observed in a limited number of cases due to the lower counting statistics of the high-energy  $\gamma$ -ray spectra and to Porter-Thomas fluctuations. However, the assignments obtained in this way play the important role of confirming and validating assignments obtained from the other methods described above.

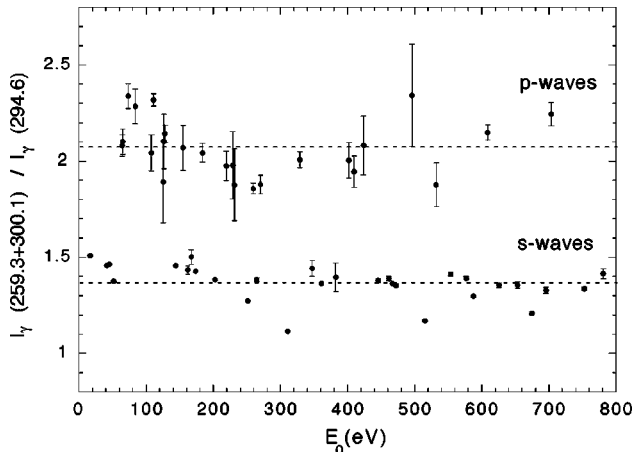


FIG. 8. Intensity ratios between the indicated  $\gamma$ -ray transitions plotted versus neutron energy for  $s$ - and  $p$ -wave resonances in  $^{107}\text{Ag}$ . The dotted lines are the means of the various groups.

TABLE I. Neutron resonance parameters for  $^{107}\text{Ag}$ .

$E$ (eV)	$g\Gamma_n$ (meV)	$l$	$J$	$A_0$ ( $\text{eV}^{-1}$ )	$A_1$ ( $\text{eV}^{-1}$ )
-11.1		0	1		
$16.3 \pm 0.02$	$2.9 \pm 0.2$	0	0		
$18.9 \pm 0.02^a$	$(1.1 \pm 1.5)10^{-4}$	1			
$20.3 \pm 0.02^a$	$(1.2 \pm 0.6)10^{-4}$	1			
$35.84 \pm 0.03^a$	$(3.4 \pm 0.5)10^{-4}$	1		12.4	30.0
$41.57 \pm 0.05$	$2.8 \pm 0.4$	0	1		
$42.81 \pm 0.03^a$	$(4.9 \pm 1.1)10^{-3}$	1			
$44.90 \pm 0.03$	$0.62 \pm 0.1$	0	1		
$51.56 \pm 0.05$	$17.9 \pm 1.8$	0	1		
$64.24 \pm 0.05^a$	$0.018 \pm 0.002$	1	1		5.2
$64.74 \pm 0.05^a$	$0.013 \pm 0.001$	1	2		
$73.21 \pm 0.06^a$	$0.027 \pm 0.006$	1	1		
$83.55 \pm 0.07$	$0.015 \pm 0.002$	1	2	0.0	0.0
$101.2 \pm 0.1^a$	$0.004 \pm 0.003$	1			
$107.6 \pm 0.1^a$	$0.014 \pm 0.002$	1	1		2.2
$110.8 \pm 0.1^a$	$0.081 \pm 0.009$	1	2	0.0	0.0
$125.1 \pm 0.1^a$	$0.010 \pm 0.001$	1	0	2.7	
$126.1 \pm 0.1^a$	$0.018 \pm 0.002$	1	1		1.7
$128.5 \pm 0.1$	$0.092 \pm 0.009$	1	2	0.0	0.0
$136.7 \pm 0.1^a$	$0.028 \pm 0.003$	1			
$141.5 \pm 0.1^a$	$0.010 \pm 0.001$	1			
$144.2 \pm 0.1$	$4.0 \pm 0.8$	0	0		
$154.8 \pm 0.1$	$0.025 \pm 0.003$	1	1		2.3
$162.0 \pm 0.2$	$0.28 \pm 0.02$	0	1		
$166.9 \pm 0.2$	$0.19 \pm 0.01$	0	0		
$173.7 \pm 0.2$	$5.50 \pm 0.5$	0	1		
$183.5 \pm 0.2^a$	$0.13 \pm 0.01$	1	1		1.8
$201.0 \pm 0.2^a$	$0.27 \pm 0.02$	1		0.18	9.8
$202.6 \pm 0.2$	$12.90 \pm 0.5$	0	1		
$218.9 \pm 0.2$	$0.084 \pm 0.008$	1	1		1.9
$228.3 \pm 0.2^a$	$0.040 \pm 0.004$	1	2		
$231.0 \pm 0.2^a$	$0.052 \pm 0.004$	1	2		
$235.5 \pm 0.2^a$	$0.029 \pm 0.004$	1			
$251.3 \pm 0.3$	$16.0 \pm 4$	0	1		
$259.9 \pm 0.3$	$0.25 \pm 0.03$	1	1		2.5
$264.5 \pm 0.3$	$2.5 \pm 0.2$	0	1		
$269.9 \pm 0.4$	$0.20 \pm 0.02$	1	1		1.8
$310.8 \pm 0.4$	$65 \pm 15$	0	1		
$328.2 \pm 0.4$	$0.60 \pm 0.10$	1	2		
$346.8 \pm 0.4$	$0.40 \pm 0.04$	0	1		
$359.7 \pm 0.4^a$	$0.26 \pm 0.1$	1			
$361.2 \pm 0.4$	$15.5 \pm 1.0$	0	1		
$372.5 \pm 0.5$	$0.19 \pm 0.02$	1			
$381.8 \pm 0.5$	$0.29 \pm 0.03$	0	1		
$384.9 \pm 0.5^a$	$0.10 \pm 0.04$	1			
$403.9 \pm 0.5$	$0.30 \pm 0.08$	1	1		
$409.2 \pm 0.5$	$0.36 \pm 0.05$	1	2		
$422.5 \pm 0.6^a$	$0.18 \pm 0.02$	1	0	1.1	
$444.0 \pm 0.6$	$21.3 \pm 2.0$	0	0		
$460.9 \pm 0.6$	$18.0 \pm 2.0$	0	1		
$466.8 \pm 0.6$	$63.0 \pm 5.0$	0	1		
$472.4 \pm 0.6$	$14.0 \pm 1.2$	0	0		
$479.3 \pm 0.7$	$0.46 \pm 0.10$	1			
$494.9 \pm 0.7^a$	$0.40 \pm 0.08$	1	2		

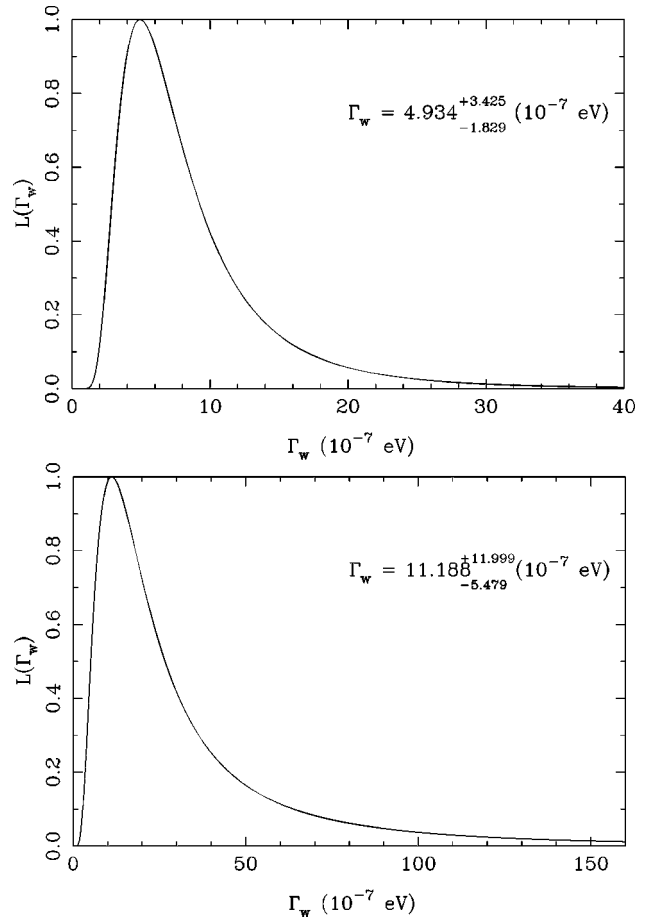
<sup>a</sup>New resonances.

TABLE II. Neutron resonance parameters for  $^{109}\text{Ag}$ .

$E$ (eV)	$g\Gamma_n$ (meV)	$l$	$J$	$A_0$ ( $\text{eV}^{-1}$ )	$A_1$ ( $\text{eV}^{-1}$ )
$5.19 \pm 0.01$	$9.5 \pm 0.3$	0	1		
$30.6 \pm 0.02$	$5.4 \pm 0.5$	0	1		
$32.7 \pm 0.03^a$	$0.013 \pm 0.002$	1	1		20.5
$40.3 \pm 0.04$	$4.4 \pm 0.4$	0	1		
$55.8 \pm 0.04$	$5.4 \pm 0.5$	0	0		
$71.0 \pm 0.04$	$18.9 \pm 1.8$	0	1		
$78.5 \pm 0.06^a$		1			
$79.8 \pm 0.06^a$		1			
$82.5 \pm 0.06$	$0.016 \pm 0.002$	1	2	0.0	0.0
$87.7 \pm 0.1$	$4.10 \pm 0.3$	0	1		
$91.5 \pm 0.1$	$0.029 \pm 0.003$	1	2	0.0	0.0
$106.3 \pm 0.1$	$0.14 \pm 0.015$	0	0		
$113.5 \pm 0.1$	$0.017 \pm 0.004$	1	2	0.0	0.0
$133.9 \pm 0.1$	$69.1 \pm 6.0$	0	1		
$139.6 \pm 0.1$	$1.50 \pm 0.5$	0	1		
$160.3 \pm 0.2^a$	$0.04 \pm 0.01$	1	1		5.7
$164.3 \pm 0.2^a$	$0.014 \pm 0.005$	1	2	0.0	0.0
$169.8 \pm 0.2$	$0.36 \pm 0.06$	1	0		
$173.1 \pm 0.2$	$33.7 \pm 3.0$	0	1		
$199.0 \pm 0.2^a$	$0.11 \pm 0.02$	1	1		3.1
$209.2 \pm 0.2$	$18.6 \pm 2.0$	0	1		
$219.2 \pm 0.2^a$	$0.06 \pm 0.008$	1	2	0.0	0.0
$251.2 \pm 0.2$	$4.4 \pm 0.4$	0	1		
$259.0 \pm 0.3$	$3.4 \pm 0.3$	0	0		
$264.7 \pm 0.3$		1	2		
$272.4 \pm 0.3$	$1.5 \pm 0.2$	0	1		
$275.8 \pm 0.3^a$	$0.054 \pm 0.006$	1			
$284.0 \pm 0.3^a$	$0.28 \pm 0.03$	1	2		
$290.6 \pm 0.3$	$8.3 \pm 0.8$	0	1		
$293.3 \pm 0.3$	$0.30 \pm 0.04$	1	1		5.2
$300.9 \pm 0.4$	$1.5 \pm 0.2$	0	0		
$316.2 \pm 0.4$	$150.0 \pm 15.0$	0	1		
$322.1 \pm 0.4$	$0.11 \pm 0.015$	1			
$327.8 \pm 0.4$	$0.65 \pm 0.07$	0	1		
$340.2 \pm 0.4$	$0.33 \pm 0.03$	1	2		
$351.4 \pm 0.4^a$	$0.055 \pm 0.006$	1	2		
$360.4 \pm 0.5^a$		0	1		
$374.5 \pm 0.5^a$		1	2		
$386.2 \pm 0.5$	$41.5 \pm 2.0$	0	1		
$391.6 \pm 0.5$	$0.16 \pm 0.02$	1	1		
$397.3 \pm 0.5$	$10.0 \pm 1.5$	0	1		
$401.7 \pm 0.5$	$42.0 \pm 5.0$	0	0		

<sup>a</sup>New resonances.TABLE III. Spacings and strength functions for  $^{107}\text{Ag}$  and  $^{109}\text{Ag}$ .

	$^{107}\text{Ag}$		$^{109}\text{Ag}$	
	current	[37]	current	[37]
$D_0$ (eV)	$25 \pm 3$	$16 \pm 3$	$21 \pm 2$	$14 \pm 2$
$S_0$ ( $10^{-4}$ )	$0.50 \pm 0.15$	$0.38 \pm 0.07$	$0.84 \pm 0.23$	$0.46 \pm 0.15$
$S_1$ ( $10^{-4}$ )	$3.5 \pm 0.8$	$3.8 \pm 0.6$	$2.8 \pm 0.8$	$3.8 \pm 0.6$

FIG. 9. Likelihood function  $L$  versus square root of the weak spreading width  $\Gamma_w$  for  $p$ -wave resonances in  $^{107}\text{Ag}$ : (top)  $L$  with spin information included and (bottom)  $L$  without the spin information.TABLE IV. Longitudinal PNC asymmetries for neutron resonances in  $^{107}\text{Ag}$ .

$E_n$ (eV)	$p$ (%)	$p/\delta p$	$J$
35.84	$-4.050 \pm 0.380$	-10.7	(0,1)
64.24	$0.135 \pm 0.060$	2.3	1
83.55	$0.027 \pm 0.043$	0.6	2
107.6	$0.390 \pm 0.060$	6.5	1
110.8	$-0.004 \pm 0.016$	-0.1	2
125.1	$0.871 \pm 0.110$	7.9	0
126.1	$0.050 \pm 0.058$	0.9	1
128.5	$0.022 \pm 0.017$	0.3	2
154.8	$-0.400 \pm 0.095$	-4.2	1
183.5	$-0.003 \pm 0.049$	-0.1	1
201.0	$-0.107 \pm 0.022$	-4.9	1 <sup>a</sup>
218.9	$0.037 \pm 0.067$	0.6	1
259.9	$0.308 \pm 0.038$	8.1	1
269.9	$0.120 \pm 0.036$	3.3	1
422.5	$0.550 \pm 0.083$	6.6	0

<sup>a</sup> $J$  deduced as explained in the text.

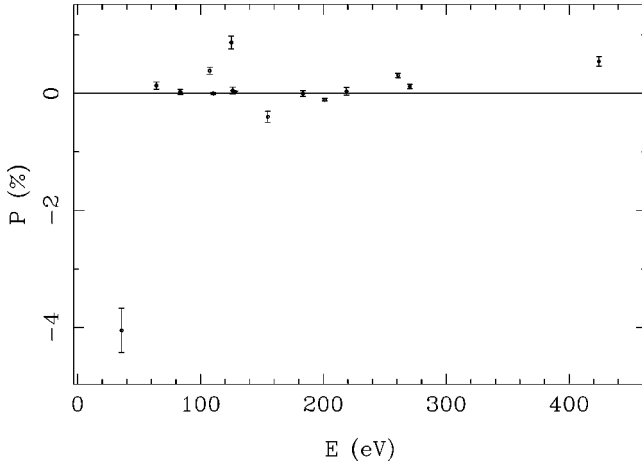


FIG. 10. Longitudinal asymmetries versus energies of neutron resonances in  $^{107}\text{Ag}$ .

#### IV. RESONANCE ANALYSIS

Our analysis to determine the resonance parameters was reported earlier [28]. This analysis was based on a transmission measurement with natural silver and a capture study (of the total  $\gamma$ -ray yield) with an enriched  $^{107}\text{Ag}$  target at LANSCE. Preliminary detailed  $\gamma$ -ray spectra were available from a capture study at IRMM on an enriched  $^{109}\text{Ag}$  target. Since this original resonance analysis, a similar capture study with the enriched  $^{107}\text{Ag}$  target was performed at IRMM, and the analysis of the  $^{109}\text{Ag}$  data was completed. The information on spin and parity assignments from the IRMM capture studies [14,29] has been combined with the resonance energies and strengths determined from the LANSCE measurements. The primary changes from the earlier work [28] are in  $^{107}\text{Ag}$ , where there are now spin assignments for most of the resonances. This is important for the PNC analysis but otherwise has relatively little effect. In a limited number of cases, there were changes in the orbital angular momentum assignments. Resonance parameters are listed in Tables I and II. The resonance energy, neutron width, orbital angular momentum  $l$ , and total angular momentum  $J$  are given for all resonances, while the quantity  $A$  (defined in the next section) is listed for those  $p$ -wave resonances for which the longitudinal asymmetry was measured. The measured values of the average level spacings and the strength functions are listed in Table III. The values for the  $s$ -wave spacings were determined from linear fits to the cumulative number of levels up to a neutron energy of 700 eV [14,29].

#### V. PARITY VIOLATION ANALYSIS

*General.* The details of the analysis approach are given by Bowman *et al.* [30]. Consider a target with spin and parity  $I^\pi$  ( $I \neq 0$ ). The  $s$ -wave levels can have  $(I \pm 1/2)^\pi$ , while the  $p$ -wave levels can have  $(I \pm 1/2)^{-\pi}$  or  $|I \pm 3/2|^{-\pi}$ . The observed asymmetry for a given  $p$ -wave level  $\mu$  has contributions from several  $s$ -wave levels  $\nu$ . The asymmetry  $p_\mu$  is [31–34]

$$p_\mu = 2 \sum_{\nu: J_\nu = J_\mu} \frac{V_{\mu\nu}}{E_\nu - E_\mu} \sqrt{\frac{\Gamma_{\nu n}}{\Gamma_{\mu n}}} \frac{g_{\mu 1/2}}{\sqrt{g_{\mu 1/2}^2 + g_{\mu 3/2}^2}}, \quad (4)$$

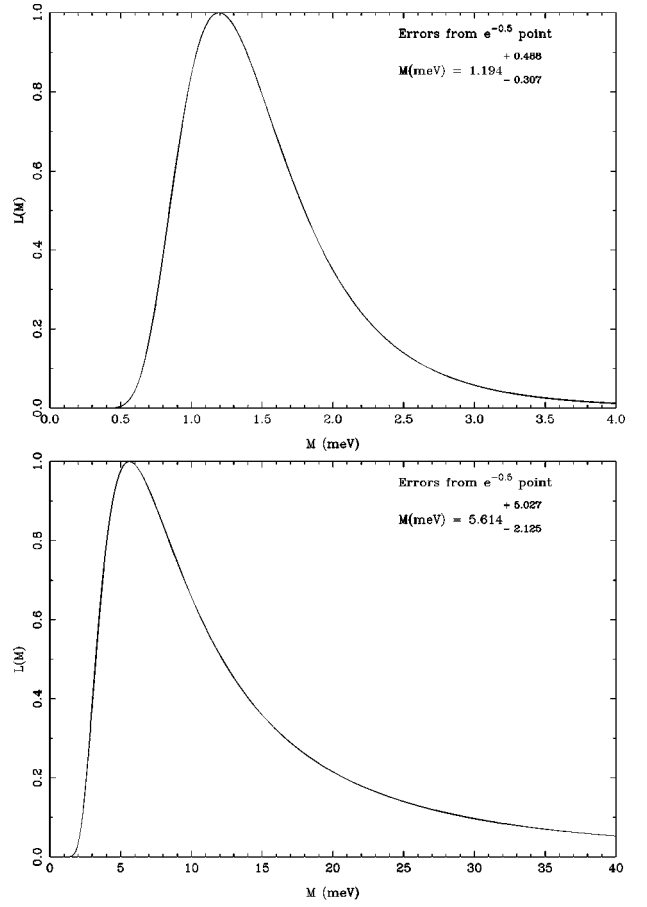


FIG. 11. (Top) Maximum likelihood plot for  $J=1$  resonances in  $^{107}\text{Ag}$ . (Bottom) Maximum likelihood plot for  $J=0$  resonances in  $^{107}\text{Ag}$ . For the calculations shown in this figure the 35.8-eV resonance was assumed to have  $J=0$ .

where  $g_{\mu 1/2}$  and  $g_{\mu 3/2}$  are the projectile-spin ( $j=1/2$  and  $3/2$ ) neutron amplitudes of level  $\mu$  ( $g_\mu^2 = \Gamma_{\mu n}$ ),  $E_\mu$  and  $E_\nu$  are the corresponding resonance energies, and  $V_{\mu\nu}$  is the matrix element of the parity violating interaction between levels  $\mu$  and  $\nu$ . Only the  $g_{1/2}$  amplitude contributes to the parity violation. According to the statistical model of the compound nucleus, the (signed) quantities  $V_{\mu\nu}$ ,  $g_\mu$ , and  $g_\nu$  are statistically independent random variables and have mean-zero Gaussian distributions [35]. The quantity  $p_\mu$  is a sum of Gaussian random variables, the  $V_{\mu\nu}$ 's, and is itself a Gaussian random variable [36]. The common variance  $M^2$  of the PNC matrix elements is the mean square matrix element of the PNC interaction. We assume that the values of asymmetries measured for different  $p$ -wave resonances have mean zero and are statistically independent.

The physics of our approach lies in the assumed form of the probability density functions for the rms parity-violating matrix element [30]. Given the appropriate likelihood function [36], the maximum likelihood estimate (MLE), or  $m_L$ , is obtained by finding the value of  $m$  that maximizes  $L(m)$ . A confidence interval for  $m_L$  can be obtained by solving the equation

$$\ln \left[ \frac{L(m_\pm)}{L(m_L)} \right] = \frac{1}{2}. \quad (5)$$

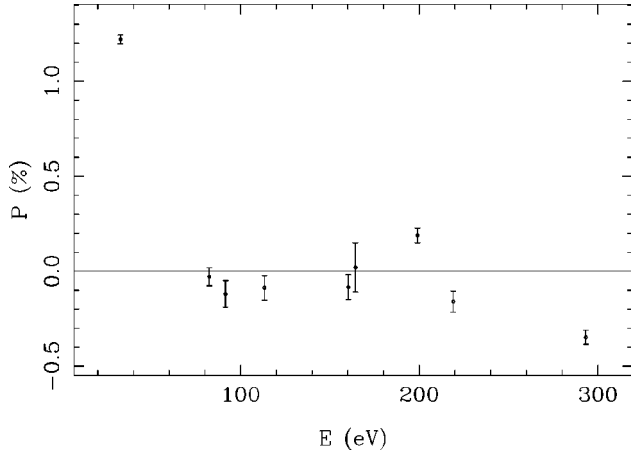


FIG. 12. Longitudinal asymmetries versus energies of neutron resonances in  $^{109}\text{Ag}$ .

If there is complete knowledge of the spectroscopic properties of the  $p$ -wave level and the nearby  $s$ -wave levels, then  $L(m)$  is determined. If the spins are unknown, then we deal explicitly with the uncertain level spins in formulating the likelihood function. For a large number of unknown resonances, this gives many terms in the sum in the likelihood expression.

Often the spins of the  $s$ -wave resonances are known, but not the spin of the  $p$ -wave level. If the spin of the  $p$ -wave level is assumed, then the coefficients of the mixing matrix element  $V_{\mu\nu}$  in Eq. (4) [which we label  $A_{\mu,\nu} = [2/(E_\nu - E_\mu)]\sqrt{\Gamma_{\nu n}/\Gamma_{\mu n}}$ ] can be evaluated. The ratio of the projectile-spin amplitudes is considered separately. The combination  $A_{\mu J}^2 = \sum_\nu A_{\mu,\nu}^2$  is used in the likelihood analysis. If  $J$  is not known, then  $A_{\mu J} = A_\mu(J)$  depends on the spin sequence assumed because only  $s$ -wave levels with the same spin as the  $p$ -wave level mix to produce parity violation. The likelihood function is then obtained by summing over  $p$ -wave level spins. Since the resonance spins for silver are

TABLE V. Longitudinal PNC asymmetries for neutron resonances in  $^{109}\text{Ag}$ .

$E_n$ (eV)	$p$ (%)	$p/\delta p$	$J$
32.70	$1.220 \pm 0.023$	53.0	1
82.50	$-0.030 \pm 0.047$	-0.6	2
91.50	$-0.120 \pm 0.070$	-1.7	2
113.5	$-0.088 \pm 0.065$	-1.4	2
160.3	$-0.084 \pm 0.065$	-1.3	1
164.3	$0.020 \pm 0.130$	0.2	2
199.0	$0.188 \pm 0.039$	4.8	1
219.2	$-0.162 \pm 0.053$	-3.0	2
293.3	$-0.348 \pm 0.037$	-9.4	1

known, one can consider the  $J=I \pm 1/2$  states separately and admit the possibility that the rms PNC matrix element  $M$  may be different for  $J=I \pm 1/2$  states. We therefore label the rms PNC matrix element as  $M_J$ . One can fit directly to the spreading width  $\Gamma_w = 2\pi M_J^2/D(J)$ , which we assume is independent of  $J$ . The likelihood function can be expressed as a function of the weak spreading width through the relation  $M_J = [\Gamma_w D(J)/2\pi]^{1/2}$ ,

$$L(\Gamma_w) = \prod_\mu \left[ \sum_{J=I \pm 1/2} P^0(M_J) p(J) P^I[q|M_J A_\mu(J), a, \sigma_\mu] + \sum_{J=I \pm 3/2} p(J) G(p_\mu, \sigma_\mu^2) \right], \quad (6)$$

where  $P^0(M_J)$  is the assumed *prior* probability density function for  $M_J$ ,  $p(J)$  is the relative probability of spin  $J$ ,  $G(p_\mu, \sigma_\mu^2)$  is a Gaussian with experimental asymmetry  $p_\mu$  and corresponding uncertainty  $\sigma_\mu$ , the quantity  $a^2$  is the ratio of the  $p_{1/2}$  and  $p_{3/2}$  strength functions, and  $P^I$  is the appropriate probability density function. However, in our

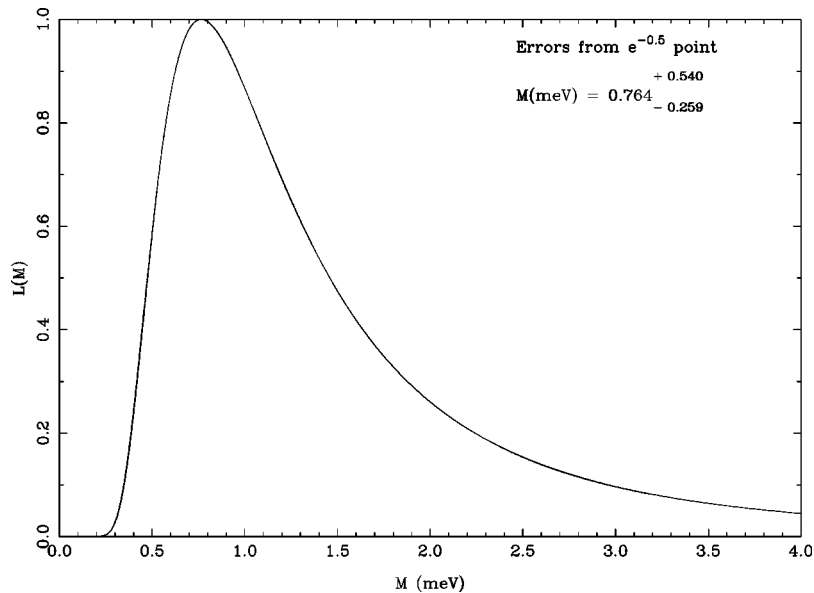


FIG. 13. Maximum likelihood plot for  $J=1$   $p$ -wave resonances in  $^{109}\text{Ag}$ .

case, since we know the spins of the resonances, we can fit separately to the matrix elements  $M_J$  using equation

$$L(M_J) = \prod_{\mu} \{P^0(M_J) P^I[q|M_J A_{\mu}(J), a, \sigma_{\mu}]\}. \quad (7)$$

Even in this favorable case, with all spins known, there is still the problem that the entrance channel neutron  $j=3/2$  and  $j=1/2$  amplitudes are unknown. This factor is accounted for statistically using the average value of the ratio of  $S_{3/2}$  and  $S_{1/2}$  strength functions. The details of this formulation are given by Bowman *et al.* [30].

## VI. RESULTS

### A. $^{107}\text{Ag}$

As noted above, information on the resonance spins is important in the determination of the rms PNC matrix element, or of the corresponding weak spreading width. For  $^{107}\text{Ag}$  the spins of the  $s$ -wave resonances are well known, and the spins of many of the  $p$ -wave resonances have been determined recently by Zanini *et al.* [14,29]. As an example, the likelihood function for  $^{107}\text{Ag}$  is shown in Fig. 9 with the information on the  $p$ -wave resonance spins included and omitted.

The values of the longitudinal asymmetries determined for  $p$ -wave resonances in  $^{107}\text{Ag}$  are listed in Table IV. Note that for this spin-1/2 target only resonances with spin  $J=0$  or  $J=1$  can show parity violation. There were two  $p$ -wave resonances without spin assignments. The resonance at 201 eV shows a statistically significant PNC effect and therefore must have  $J=0$  or  $J=1$ . Since most of the  $s$ -wave cross section at the  $p$ -wave resonance is due to  $s$ -wave resonances with  $J=1$ , we assign  $J=1$  to the 201-eV resonance. The other  $p$ -wave resonance with unknown spin is located at 35.8 eV. Since this resonance shows a strong PNC effect, it cannot have  $J=2$ . There is no strong evidence to choose between  $J=0$  and  $J=1$ . We therefore calculated the rms PNC matrix element in three ways: omitting the 35.8-eV resonance, including this resonance with a  $J=0$  assignment, and including this resonance with a  $J=1$  assignment.

Figure 10 shows a plot of the longitudinal asymmetries  $p$  versus energy  $E$ . Maximum likelihood plots are shown for  $J=1$  and for  $J=0$  in Fig. 11. For the calculations shown in this figure the 35.8-eV resonance is assumed to have  $J=0$ . For  $^{107}\text{Ag}$  the values of the rms matrix elements (not including the 35.8-eV resonance) are  $M_{J=1} = 1.19_{-0.31}^{+0.49}$  meV and  $M_{J=0} = 6.04_{-2.61}^{+7.57}$  meV. Including the 35.8-eV resonance led only to small changes:  $M_{J=1} = 1.21_{-0.30}^{+0.46}$  meV assuming  $J=1$  and  $M_{J=0} = 5.61_{-2.13}^{+5.03}$  meV assuming  $J=0$ . The  $M_{J=0}$  value for  $^{107}\text{Ag}$  has a large uncertainty because it is obtained from only three PNC effects. Nevertheless, the  $M_J$  values for  $^{107}\text{Ag}$  appear to demonstrate for the first time a  $J$  dependence of  $M_J$ .

The spreading width of the PNC interaction is  $\Gamma_w = 2\pi M_J^2/D_J$ . The level spacings of these  $I=1/2$  targets are strongly spin-dependent, and are expected to follow approximately a  $(2J+1)^{-1}$  dependence. Therefore the average size

of the matrix element should depend on the level density. Assuming a  $(2J+1)^{-1}$  spacing dependence and using the observed  $s$ -wave level spacing of 25 eV, yields  $D_{J=1} = 33.3$  eV. The value of  $\Gamma_w$  for the  $J=1$  states is  $\Gamma_w = (2.67_{-1.21}^{+2.65}) \times 10^{-7}$  eV. The likelihood analysis also was performed with the data from both spins simultaneously (assuming that  $M_J^2$  scales with  $D_J$ ), yielding  $\Gamma_w = (4.93_{-1.87}^{+3.43}) \times 10^{-7}$  eV. Although these two values for the spreading width are different by a factor of 2, they are consistent within the large uncertainty associated with each value, and therefore do not contradict the hypothesis that the spreading width is independent of  $J$ .

### B. $^{109}\text{Ag}$

The values of the longitudinal asymmetries determined for  $p$ -wave resonances in  $^{109}\text{Ag}$  are listed in Table V. The spin assignments for the  $p$ -wave resonances are from Zanini *et al.* [14,15]. A plot of longitudinal asymmetries  $p$  versus energy  $E$  for  $^{109}\text{Ag}$  is shown in Fig. 12. The maximum likelihood plot for the  $J=1$  resonances is shown in Fig. 13, with the most likely value  $M_J = 0.76_{-0.26}^{+0.54}$  meV. For  $^{109}\text{Ag}$  the observed  $s$ -wave level spacing is  $D_J = 21$  eV, which leads to  $D_{J=1} = 28$  eV. For  $J=1$  the corresponding value for  $\Gamma_w = (1.30_{-0.74}^{+2.49}) \times 10^{-7}$  eV.

## VII. SUMMARY

PNC longitudinal asymmetries have been measured for 15  $p$ -wave resonances in  $^{107}\text{Ag}$  and nine  $p$ -wave resonances in  $^{109}\text{Ag}$ . A total of 12 resonances (eight in  $^{107}\text{Ag}$  and four in  $^{109}\text{Ag}$ ) show parity violation with greater than  $3\sigma$  statistical significance. Of these 12 resonances seven have positive signs and five have negative signs (relative to the sign of the PNC effect at 0.73 eV in  $^{139}\text{La}$  [1]). These results are consistent with a statistical distribution of the signs of the PNC effects, and provide additional evidence that the sign correlation observed in  $^{232}\text{Th}$  [12] is a property of  $^{232}\text{Th}$  and is not generic. With all resonance spins known, the values of the rms matrix elements  $M_J$  for the two nuclides were determined directly. Our data suggest that the rms parity-violating matrix element depends on the resonance spin. The values of the weak spreading widths (in the range  $1-5 \times 10^{-7}$  eV) are approximately equal to those obtained in  $^{232}\text{Th}$  and  $^{238}\text{U}$ , and thus consistent with a constant weak spreading width. More measurements in this mass region are required to establish definitively the mass dependence of the weak spreading width.

## ACKNOWLEDGMENTS

This work was supported in part by the U.S. Department of Energy, Office of High Energy and Nuclear Physics, under Grants No. DE-FG02-97-ER41042 and DE-FG02-97-ER41033, and by the U.S. Department of Energy, Office of Energy Research, under Contract No. W-7405-ENG-36.

- [1] V. P. Alfimenkov, S. B. Borzakov, Vo Van Thuan, Yu. D. Mareev, L. B. Pikelner, A. S. Khrykin, and E. I. Sharapov, *Nucl. Phys.* **A398**, 93 (1983).
- [2] E. G. Adelberger and W. C. Haxton, *Annu. Rev. Nucl. Part. Sci.* **35**, 501 (1985).
- [3] B. Desplanques, J. F. Donoghue, and B. R. Holstein, *Ann. Phys. (N.Y.)* **124**, 449 (1989).
- [4] J. D. Bowman, G. T. Garvey, Mikkel B. Johnson, and G. E. Mitchell, *Annu. Rev. Nucl. Part. Sci.* **43**, 829 (1993).
- [5] C. M. Frankle, S. J. Seestrom, N. R. Roberson, Yu. P. Popov, and E. I. Sharapov, *Phys. Part. Nuclei* **24**, 401 (1993).
- [6] V. V. Flambaum and G. F. Gribakin, *Prog. Part. Nucl. Phys.* **35**, 423 (1995).
- [7] J. D. Bowman *et al.*, *Phys. Rev. Lett.* **65**, 1192 (1990).
- [8] X. Zhu *et al.*, *Phys. Rev. C* **46**, 768 (1992).
- [9] C. M. Frankle *et al.*, *Phys. Rev. Lett.* **67**, 564 (1991).
- [10] C. M. Frankle *et al.*, *Phys. Rev. C* **46**, 778 (1992).
- [11] B. E. Crawford *et al.*, *Phys. Rev. C* **58**, 1225 (1998).
- [12] S. L. Stephenson *et al.*, *Phys. Rev. C* **58**, 1236 (1998).
- [13] L. Y. Lowie, Ph.D. thesis, North Carolina State University, 1996.
- [14] L. Zanini, Ph.D. thesis, Delft University, 1998.
- [15] L. Zanini, F. Corvi, K. Athanassopoulos, H. Postma, and F. Gunsing, in *Capture Gamma-Ray Spectroscopy and Related Topics*, edited by G. L. Molnar, T. Belgia, and Zs. Revay (Springer, Budapest, 1997), p. 379.
- [16] F. Corvi, L. Zanini, H. Postma, and F. Gunsing, in *Nuclear Data for Science and Technology*, edited by G. Reffo, A. Ventura, and C. Grandi (Editrice Compositori, Bologna, 1997), p. 734.
- [17] P. W. Lisowski, C. D. Bowman, G. J. Russell, and S. A. Wender, *Nucl. Sci. Eng.* **106**, 208 (1990).
- [18] N. R. Roberson *et al.*, *Nucl. Instrum. Methods Phys. Res. A* **326**, 549 (1993).
- [19] J. J. Szymanski *et al.*, *Nucl. Instrum. Methods Phys. Res. A* **340**, 564 (1994).
- [20] S. I. Penttila, J. D. Bowman, P. P. J. Delheij, C. M. Frankle, D. G. Haase, R. Mortensen, H. Postma, S. J. Seestrom, and Yi-Fen Yen, in *Time Reversal Invariance and Parity Violation in Neutron Resonances*, edited by C. R. Gould, J. D. Bowman, and Yu. P. Popov (World Scientific, Singapore, 1994), p. 198.
- [21] S. I. Penttila, J. D. Bowman, P. P. J. Delheij, C. M. Frankle, D. G. Haase, H. Postma, S. J. Seestrom, and Yi-Fen Yen, in *High Energy Spin Nuclear Physics*, edited by K. J. Heller and S. L. Smith (American Institute of Physics, New York, 1995), p. 532.
- [22] V. W. Yuan *et al.*, *Phys. Rev. C* **44**, 2187 (1991).
- [23] J. D. Bowman, S. I. Penttila, and W. B. Tipples, *Nucl. Instrum. Methods Phys. Res. A* **369**, 195 (1996).
- [24] Yi-Fen Yen *et al.*, in *Time Reversal Invariance and Parity Violation in Neutron Resonances*, edited by C. R. Gould, J. D. Bowman, and Yu. P. Popov (World Scientific, Singapore, 1994), p. 210.
- [25] J. D. Bowman, Y. Matsuda, B. E. Crawford, and Y.-F. Yen (unpublished).
- [26] C. W. Reich and M. S. Moore, *Phys. Rev.* **111**, 929 (1958).
- [27] L. M. Bollinger and G. E. Thomas, *Phys. Rev.* **171**, 1293 (1968).
- [28] L. Y. Lowie *et al.*, *Phys. Rev. C* **56**, 90 (1997).
- [29] L. Zanini, F. Corvi, H. Postma, and K. Athanassopoulos, ISINN-5, JINR Report No. E3-3-97-213 Dubna, 1997, p. 221.
- [30] J. D. Bowman, L. Y. Lowie, G. E. Mitchell, E. I. Sharapov, and Yi-Fen Yen, *Phys. Rev. C* **53**, 285 (1996).
- [31] O. P. Sushkov and V. P. Flambaum, *Pis'ma Zh. Eksp. Teor. Fiz* **32**, 377 (1980) [*JETP Lett.* **32**, 352 (1980)].
- [32] V. E. Bunakov and V. P. Gudkov, *Z. Phys. A* **303**, 285 (1981).
- [33] J. R. Vanhoy, E. G. Bilpuch, J. F. Shriner, Jr., and G. E. Mitchell, *Z. Phys. A* **331**, 1 (1988).
- [34] C. R. Gould, D. G. Haase, N. R. Roberson, H. Postma, and J. D. Bowman, *Int. J. Mod. Phys. A* **5**, 2181 (1990).
- [35] O. Bohigas and H. A. Weidenmüller, *Annu. Rev. Nucl. Part. Sci.* **38**, 421 (1988).
- [36] W. T. Eadie, D. Drijard, F. E. James, M. Roos, and B. Sadoulet, *Statistical Methods in Experimental Physics* (North-Holland, Amsterdam, 1971), p. 59.
- [37] S. F. Mughabghab, M. Divadeenam, and N. E. Holden, *Neutron Cross Sections* (Academic, New York, 1988), Vol. 1, Pt. A.